Engineering Analysis with Boundary Elements 41 (2014) 111–121

Contents lists available at ScienceDirect

Engineering Analysis with Boundary Elements

journal homepage: www.elsevier.com/locate/enganabound

Automatic thermal analysis of gravity dams with fast boundary face method

Jianming Zhang*, Cheng Huang, Chenjun Lu, Lei Han, Pan Wang, Guangyao Li

State Key Laboratory of Advanced Design and Manufacturing for Vehicle Body, Hunan University, Changsha 410082, Hunan, China

ARTICLE INFO

Article history:
Received 8 October 2013
Accepted 2 January 2014

Keywords:
Gravity dam
Boundary face method
Transient thermal analysis
Hierarchical matrix
ACA

ABSTRACT

It is well recognized that the dam's construction schedule has significant influences in long-term concrete temperature, whose variations may produce local thermal stress and thus result in damage and cracking. This paper describes a methodology for predicting the thermal evolution of dams during their construction by the boundary face method (BFM). This work involves the following aspects: (1) the BFM is integrated into the UG-NX, making the analysis performed entirely within the CAD environment; (2) two kinds of new elements, i.e. tube element and element with negative parts are proposed to deal with cooling water pipes embedded in dams; (3) a domain number sequence optimization method is proposed for multi-domain problems for the best band of the assembling system matrix; (4) a geometric mapping cross approximation (GMCA) method is proposed to make the low-rank representation of the BIE more convenient and efficient; (5) the quasi-initial condition method for transient thermal problems is implemented and a time step scaling method is proposed to solve the instability problem in case of short time steps. Benchmark examples are presented and compared with other solutions by the FEM.

1. Introduction

It is widely recognized by engineers that the high temperature generated in the concrete due to the hydration heat of the cement paste is one of the main factors that result in fractures and damage for concrete hydraulic structures during their construction. Various aspects of thermal stresses in concrete dams have been investigated and reported using finite element method (FEM), but many problems of calculating thermal stresses in concrete masses still do not have a satisfactory solution. Moreover, the results reported by different researchers are different or even contradict to each other. The reason for this may owe to that the FEM has the following intrinsic drawbacks:

(1) Many kinds of abstract element, e.g. beam element, shell element, bar element, spring element, etc., are used in the FEM. These elements are all based on some mathematic assumptions. Selection of proper element type and reasonable explanation to the computational results require sound theoretical background, good knowledge of all elements performance and rich experience in numerical analysis.
(2) The analysis automation of the FEM is presently at very low level. As the FEM model (approximate grid model) is completely different from the CAD model (continuous parametric model), not only in geometry and topology, but also in representation data structure. This makes the interaction between CAE and CAD extremely difficult.
(3) The task of proper meshing for the FEM analysis is challenging and keeps the most critical part of the analysis. To make a dam meshable, the geometry of the dam structure is often modified and simplified. In the modification, small sized features at the connecting area between different parts of the structure are simply omitted. These features, however, are most possibly the places where local stress concentrations take place and cracks originate from. Moreover, further assumptions are required to connect different kinds of elements in the assembled matrix, e.g. connection between solid and shell elements. This leads to much worse accuracy for the stresses.
(4) The FEM is based on the equivalent weak form of the governing equation and the boundary conditions of the BVP. The trial functions in the FEM formulation must be at least C1 continuous. The C1 continuity requirement for the trial function increases the difficulty of constructing the elements, especially shell and beam elements, and leads to a number of contradictions, e.g. the contradiction between conforming and non-conforming elements, accurate integration and locking problems, reduced integration and hourglass modes, accuracy and stability in penal function method, etc. It is just guaranteed that an FEM solution converges when the element size approaching zero. Therefore, errors of the FEM come from

* Corresponding author at: College of Mechanical and Vehicle Engineering, Hunan University, Changsha 410082, Hunan, China. Tel.: +86731 88823061.
E-mail address: zhangjm@hnu.edu.cn (J. Zhang).

0955-7997/$ - see front matter © 2014 Elsevier Ltd. All rights reserved.
http://dx.doi.org/10.1016/j.enganabound.2014.01.001

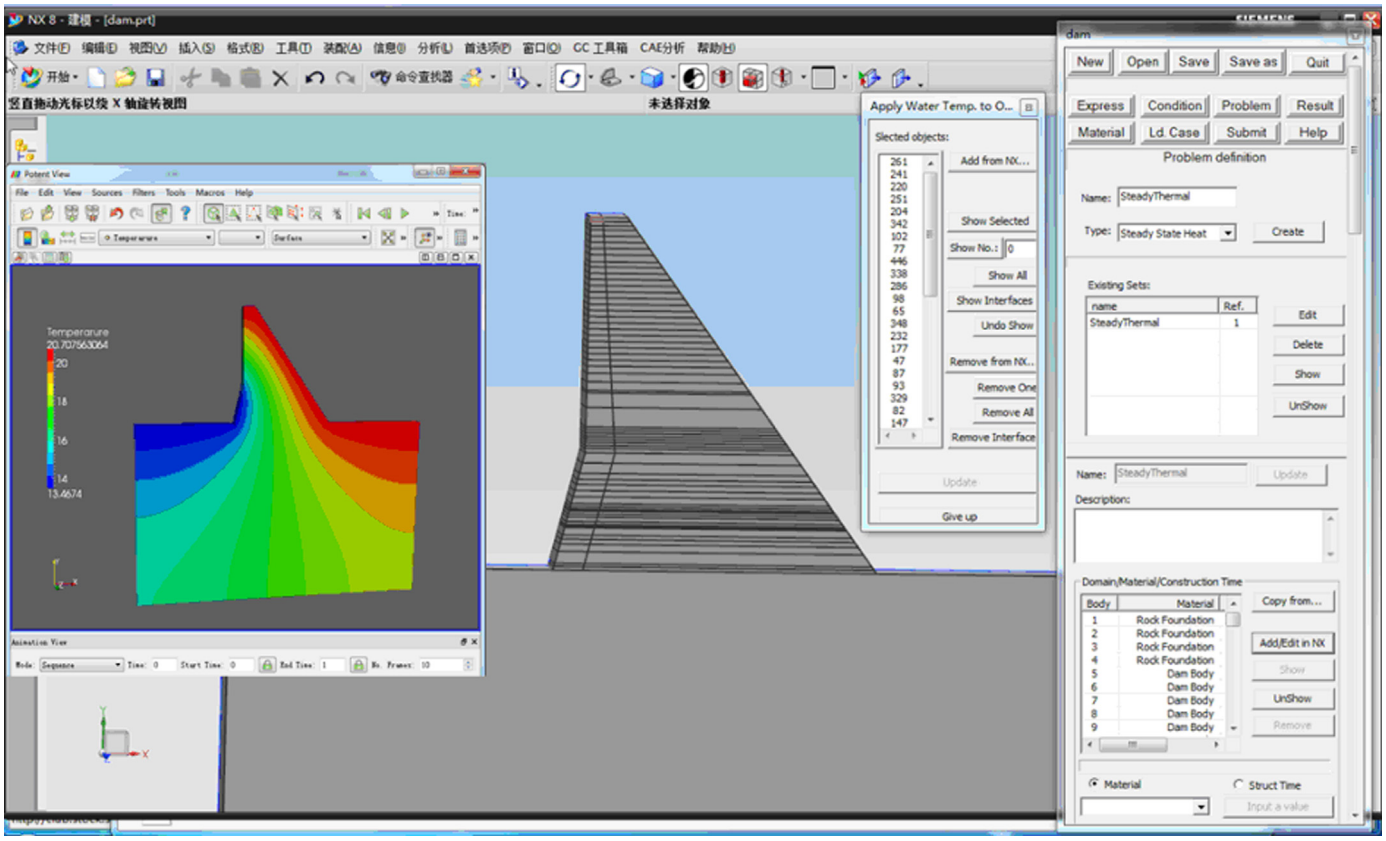

Fig. 1. UI of the Potent 1.0.

not only the approximation of the trial function but also from the "weak form" theory. Meanwhile, for a stress analysis by FEM, as stresses are calculated from the derivatives of displacements, the accuracy for stresses is lower by one order than displacements. In many cases, however, engineers are more concerned by the stress values.

To overcome the above problems, we have put forward the concept of complete solid stress analysis (CSSA) [1] and proposed the boundary face method (BFM) [2,3] based on the boundary integral equation (BIE) [4–8] to carry out the CSSA. In most cases, the BFM requires only boundary mesh, which can be obtained by discretizing each piecewise continuous panel of the body's surface without restriction of element connectivity, hence, considerably simplifies the discretization task. Moreover, it uses the parametric representation of domain surfaces, only. Such representation is used in any CAD software and can be accessed in commercial packages via Open Architecture features (usually the in-process COM servers/objects can be exploited). This may considerably simplify the data pre-processing and lead to substantial resources savings.

Our contributions are as follows:

1) Integrating the BFM into UG-NX, making the conductions of the analyses entirely within the CAD environment.
2) Proposing two kinds of new elements, i.e. tube element and element with negative parts. These elements have been successfully used to deal with cooling water pipes in dam.
3) Proposing a domain number sequence optimization method for solving multi-domain problems, which can deal with arbitrary inter-domain connections and get best efficiency by optimizing the band of the assembling system matrix.
4) Proposing a geometric mapping cross approximation (GMCA) method [9], which is equivalent to ACA but without iteration. The GMCA makes the low-rank representation of the BIE more convenient and efficient.
5) Implementing a quasi-initial condition method for transient thermal problems, and proposing a time step scaling method to solve the instability problem occurs in case of short time steps. (This is the case for dam simulation, as the heat conductivity of concrete is small but its hydration speed is relatively high).

2. Implementation of the BFM for dam simulation

2.1. Integration of the BFM into UG-NX

A primary version of CSSA software (Potent 1.0) has been developed. This software is completely integrated into the environment of the well known CAD package UG-NX (see Fig. 1). So far, the Potent 1.0 is able to solve problems in theories of static elasticity [10], steady state [11] and transient heat transfer [12] and acoustics [13]. Details can be found at the web site: http://www.5aCAE.com.

The Potent 1.0 is not only more accurate and efficient than most well known commercial CAE packages (e.g. NASTRAN, ANSYS, etc.), but also exhibits the following extraordinary merits:

1) Analysis can be easily performed by clicking some buttons in the UI of the NX-UG. It is not necessary for the users to master the knowledge about computational mechanics but just knowledge about material mechanics. With correctly imposed boundary conditions, accurate results can be obtained.

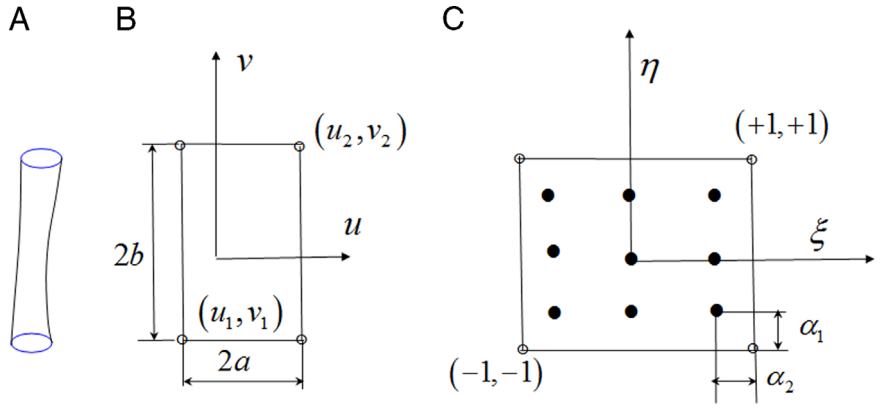

Fig. 2. Tube element.

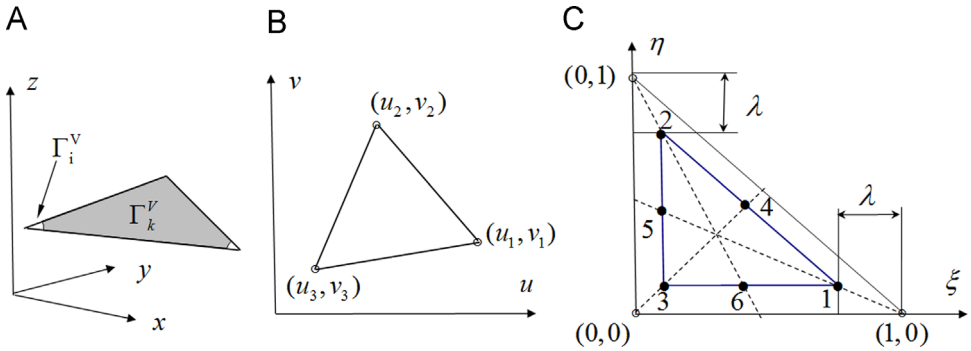

Fig. 3. A triangular element with negative parts.

2) Imposition of constraints and loads is also accomplished in the UI of the NX-UG. They are intuitively imposed on the CAD model rather than on the grid model. The mesh for the structure is automatically generated and invisible to the user. Therefore, the user does not need to care about meshing.
3) Accurate prediction of temperature at arbitrary points can be made on a complex structure, e.g. in the vicinity of the cooling water pipes. Case studies investigating how the construction schedule affects the temperature development can also be easily performed. As the analysis is conducted exactly on the same CAD model and also operated in the UI of the same CAD software, the structure can be modified quickly based on the computational results, and restart the analysis immediately. This process can be automatically repeated until an optimal schedule is achieved.

2.2. Special elements for cooling water pipes

To control the temperature development during a dam construction, a practical way is to embed cooling water pipes into some layers of the dam. The diameters of the water pipes are usually 3–4 cm, while dimensions of the dam are of hundreds of meters. Direct discretization of these pipes using traditional methods will result in prohibitive large amount of elements. This is the reason why in most FEM analysis, the specific shape and dimensions of the water pipes are simply omitted but instead, an equivalent heat sink is assumed to take into account the cooling effect of them. Obviously, the equivalent method will deteriorate the accuracy of the analysis, especially at points near the pipes. Some special hole elements have been developed to deal with the domain around the hole to achieve the purpose of mesh reduction [14–17]. To consider the exact geometry of the pipes while keeping the computational scale under control so that the analysis can be conducted on a desktop computer, we proposed two kinds of special elements: the tube element and the triangle element with negative part [11,12]. By using these special elements, the discretization of the surface is very simple, resulting in substantial savings in both data preparation and computing costs.

The tube element is shown in Fig. 2(a). The surface of the tube is mapped into a parametric space (u, v) (Fig. 2(b)), v is along tube's longitudinal direction, while u is along the circumferential direction taking a value from 0 to 2π. To perform numerical integration, a tube element is mapped into a normalized space denoted by the local coordinate system (ξ, η). A type of the discontinuous tube elements is used. There is an offset between each node and the associated element vertex. And the location of the node is determined by two offset parameters, α_1 and α_2. The shape functions M in the circumferential direction and N in the longitudinal direction are defined by Eq. (1).

$$
\begin{aligned}
&M^0(u) = \tfrac{1}{3} + \tfrac{2}{3}\cos u, \quad N^0(\beta) = -\tfrac{1}{2}\beta(1-\beta)\\
&M^1(u) = \frac{1}{3} + \frac{\sqrt{3}}{3}\sin u - \frac{1}{3}\cos u, \quad N^1(\beta) = \frac{1}{2}\beta(1+\beta)\\
&M^2(u) = \frac{1}{3} - \frac{\sqrt{3}}{3}\sin u - \frac{1}{3}\cos u, \quad N^2(\beta) = (1+\beta)(1-\beta)
\end{aligned}
\tag{1}
$$

where

$$
u = \frac{2\pi \times (\xi + 1.0)}{2} - \frac{\pi}{3}, \quad \beta = \frac{\eta}{1.0 - \alpha_2}, \quad \alpha_2 \in (0, 1).
$$

The triangle element with negative part shown in Fig. 3 is designed to deal with the tiny holes on the end faces cut by the pipes. The element is defined in the surface parametric space (u, v) by three or six vertices with parametric coordinates as shown in Fig. 3(b). And Fig. 3(c) depicts the element in the local coordinate

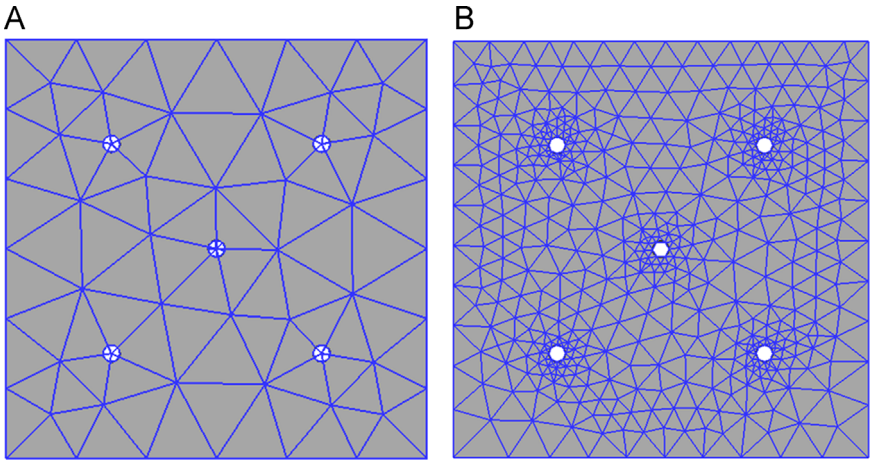

Fig. 4. A face with five small holes. (a) Triangular mesh with new elements. (b) Traditional triangular mesh.

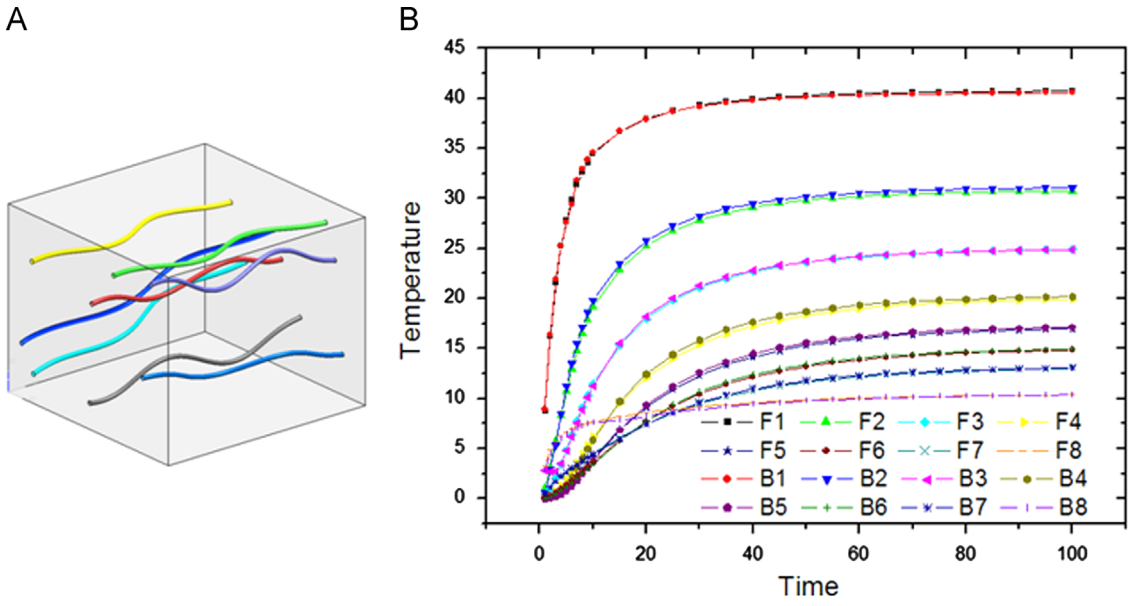

Fig. 5. Comparison with finite element method.

system (ξ, η) mapped from the space (u, v). During numerical integration, at first, the initial integrals over the whole triangular element are computed. Then, the final integrals over the surface region on the element are calculated by subtracting the integrals in all negative parts from the initial integrals. Fig. 4 shows an example of meshing on a square face with five holes by the triangle elements with negative parts and traditional triangle elements, respectively.

A validation example of a transient thermal problem solved by BFM and FEM is presented in Fig. 5. It is seen that results obtained by our method are in good agreement with that by FEM. However, the BFM computation used only 1656 nodes, while to get same level of accuracy by the FEM, 129,594 nodes are required. For details please refer [11,12].

2.3. *Domain number sequence optimization method for multi-domain problems*

Concrete gravity dams generally are composed of a number of blocks, which are filled with different types of cements and hence have different thermal properties. For the construction simulations, the dams are divided into hundreds of layers, and the numbers of layers involved in each time steps of the analysis increases in the process of the dam elevation. Therefore, a multi-domain solver [18–20] is a must for the simulation. Fortunately, a multi-domain formulation has a very beneficial advantage that

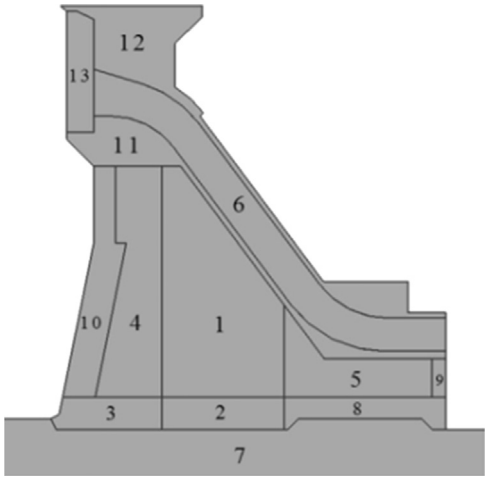

Fig. 6. Domain numbers of a concrete dam.

it leads to an overall assembled coefficient matrix in the final system equations with a sparse blocked structure. If the resultant sparsity of the matrix is fully taken advantage of, the computational efficiency can be considerably improved. The sparsity pattern is directly related to the number order of the domains. However, the domain number obtained from UG model is usually in random order. In this work, a domain number optimization method is proposed. In this algorithm, one or more level structures are generated, which are rooted at the domains of the lowest degree. For each successive structure, a value representing the bandwidth is computed. Finally, the domains are renumbered according to the level structure of the smallest bandwidth. Fig. 6 shows an example of arbitrarily connected domains of a dam. The structure is discretized with 6868 quadratic triangle and quad elements and 21,733 nodes. The optimized domain number sequence is 12, 13, 6, 11, 10, 9, 5, 4, 1, 3, 8, 2, 7, which is shown in Fig. 7. The sparsity patterns of the overall matrices before and after optimization are shown in Fig. 8. The time used for LU-decomposition of the overall matrix is 128 s and 54 s, respectively. It is seen that a big improvement of efficiency has been achieved. And it can be expected that with increasing the total number of nodes, the improvement will be more remarkable. The optimization method is similar to the node number optimization in FEM. For details please refer [21].

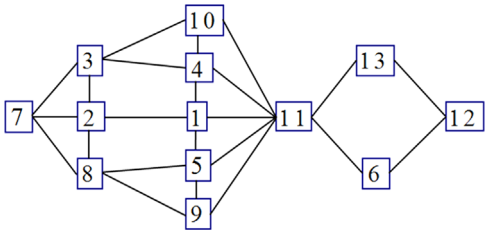

Fig. 7. Domain number sequence optimization.

2.4. Geometric mapping cross approximation method for low-rank representation

Discretization of a gravity dam may result in a large number of elements, up to millions usually, making the computational scale extremely large. The non-local kernels of the integral operator in the BIE make the situation even worse. As the coefficient matrix is fully populated, both the memory requirement and CPU time for solving the system equation are of $O(N^2)$ complexity, where N is the number of unknowns. Among the so far available accelerating methods that can dramatically reduce the memory and computational time, the hierarchical matrix (H-matrix) [22] combined with the adaptive cross approximation (ACA) [23] is a purely algebraic algorithm, and can be easily integrated into existing BEM codes. Nevertheless, even with the reduced complexity of $O(N\log N)$, the memory requirement for the H-matrix is much higher than that for the fast multipole method (FMM) [24–28]. In this work, we have implemented the basic algebraic algorithms of the H-matrix in a out-of-core manner, including addition, multiplication, inversion and LU-decomposition etc., and use the ACA to compute the low rank matrix in the H-matrix. The original ACA is an iterative algorithm, in which the involved matrix entries are calculated during the iteration. In the conventional BEM, however, the boundary integration is carried out in a way that integration quantities (Gaussian points, Jacobians, out normals etc.) are first computed, and then loop for all source nodes. Therefore, a non-iterative version of ACA that could determine the skeleton points of the low rank matrix before computing the boundary integrals would be desirable and beneficial. Besides, this version of ACA would be more convenient to insert into an existing BEM code. To this end, we proposed a geometric mapping cross approximation (GMCA) [9]. Our method is based on a geometric mapping operation, which just needs some simple geometric transformations, and determines the skeleton points before assembling the low rank approximation. By our method the procedure of low rank approximation and the evaluation of boundary integrals are separated. In contrast, the original ACA does them in one routine

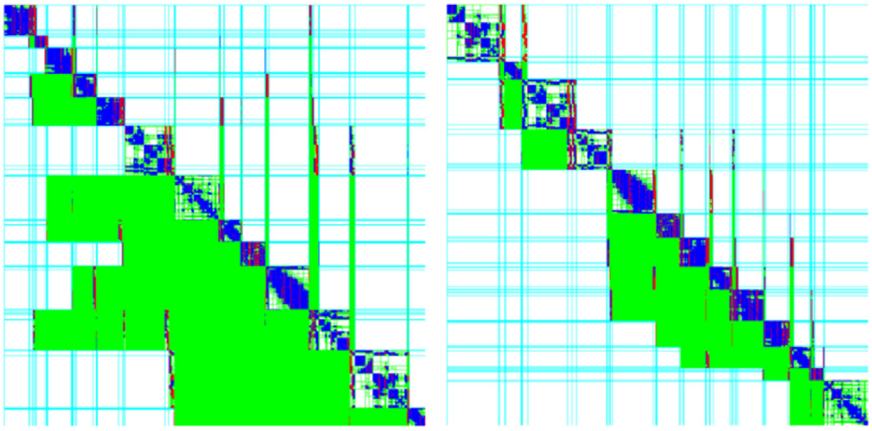

Fig. 8. The assembled overall matrices before and after optimization.

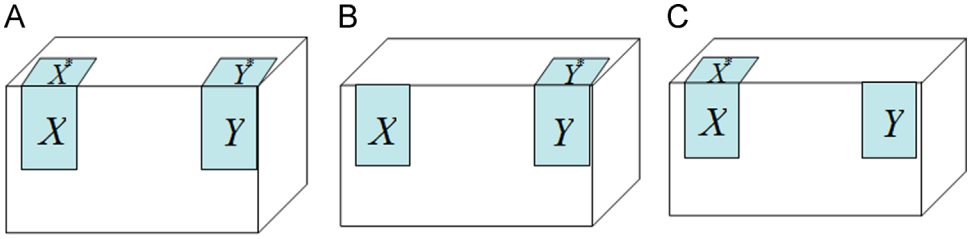

Fig. 9. Geometries for the examples with single layer potential gradients.

and, therefore, would be inconvenient and inefficient in the cases where the matrix entries need to be numerically evaluated. This is why so far most fast BEM implementations are based on constant elements. Three validation examples of the GMCA are presented in Fig. 9. In these examples, we consider the matrix **A** with entries

$$\mathbf{A}_{ij} := \frac{\langle n(x_i), x_i - y_i \rangle}{\|x_i - y_j\|} i \in m, j \in n \tag{2}$$

where the vertices $x_i \in X \cup X^*$, $y_j \in Y \cup Y^*$, are chosen as in Fig. 9, $n(x_i)$ is the outer unit normal vector to $X \cup X^*$. When X and Y lie in the same plane, the outer unit normal $n(x_i)$ and the vector drown from y_i to x_i are perpendicular. Thus, all entries $\mathbf{A}_{ij}$ with $x_i \in X$ and $y_j \in Y$ are zero.

The results are compared with the ACA in Table 1. In the table, m and n denote the numbers of the vertices in the domains X and Y, respectively. It is seen that the accuracy for some examples of the GMCA is somewhat worse than that of the ACA. However, the necessary ranks for them are less and the storage requirement can be further reduced. For details please refer [9].

2.5. Time step scaling in quasi-initial condition method of transient thermal analysis

A quasi-initial condition method has been implemented to solve the time domain boundary integral equation in the dam transient thermal analysis. Because of the high hydration speed of concrete, the time steps used in the analysis have to be relatively small. On the other hand, as the heat conductivity of concrete is very small, large time steps are necessary to maintain the computation numerically stable. To overcome this difficulty, a time step scaling method is proposed. In the proposed method, the time step is first amplified and the temperature and the fluxes are computed at the end point of the amplified step, namely a virtual time point. The boundary conditions at the virtual time point are determined through a linear interpolation using the conditions at the real time point (the end point of the real time step) and the quasi-initial time. Furthermore, the heat sources are assumed to be constant during the amplified step, which is taken as the same as that in the real time step. Finally, the temperature and the fluxes at the virtual time point are linearly interpolated back to the end point of the real time step. A theoretical verification of the time scaling method can be found in Ref. [29]. Fig. 10 shows an example of transient heat conduction in a cube. In the case that the time step equals to 0.1 s, the result is wrong. However, when the time step is amplified by 2, 4 and 8 times, the results converge to the exact solution.

Table 1
Numerical results obtained by GMCA and ACA.

Example	m	n	New algorithm		ACA	
			k	Accuracy	k	Accuracy
(a)	800	800	4	1.452×10^{-3}	5	3.885×10^{-2}
(b)	400	800	2	3.137×10^{-4}	4	4.606×10^{-6}
(c)	800	400	2	2.448×10^{-5}	4	7.943×10^{-6}

3. Results for thermal simulation of dams

Several numerical examples for thermal analysis of dams are presented and compared with other solutions by commercial FEM

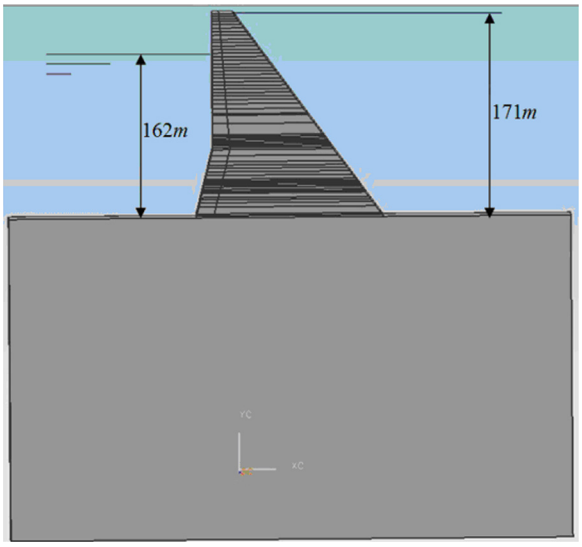

Fig. 11. The dam model defined in UG-NX.

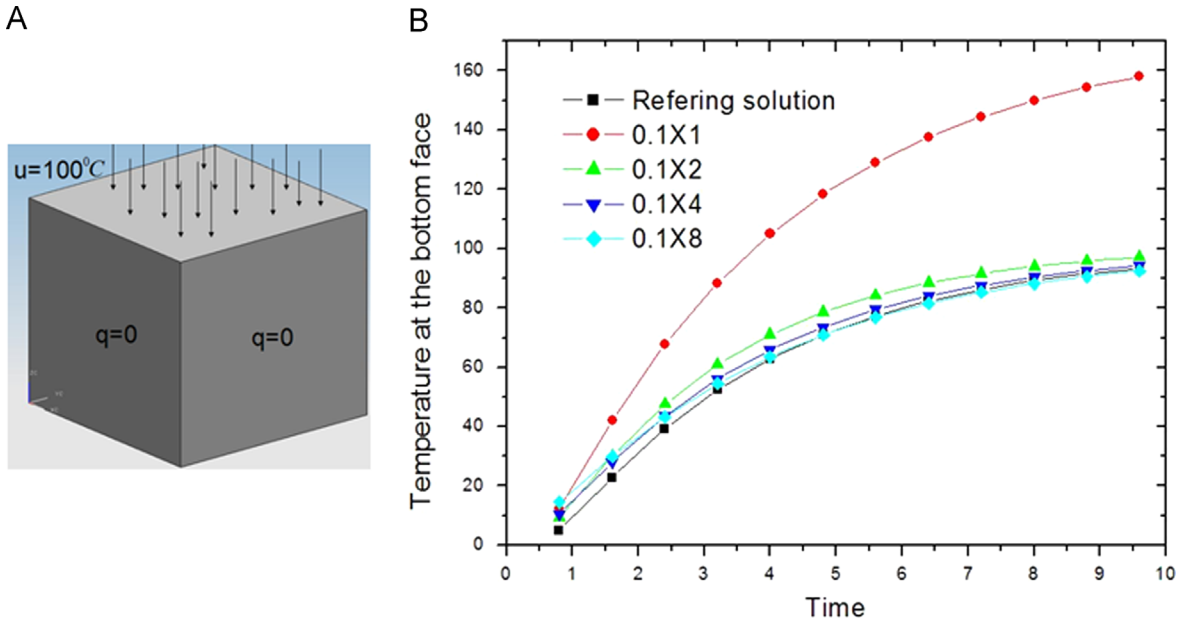

Fig. 10. Transient heat conduction in a cube.

Table 2
Material properties for the dam and rock foundation.

	c, kJ/(kg °C)	ρ, kg/m^3	κ, kJ/(m h °C)
Dam	2400	0.9627	9.27
Base	2450	0.9627	8.776

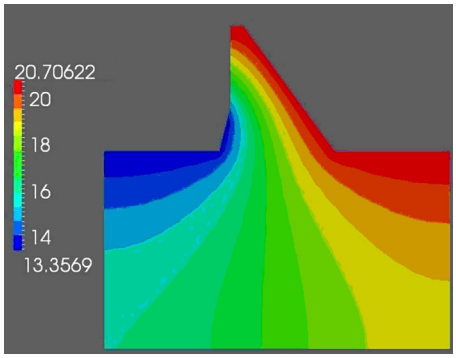

Fig. 12. The thermal state by BFM.

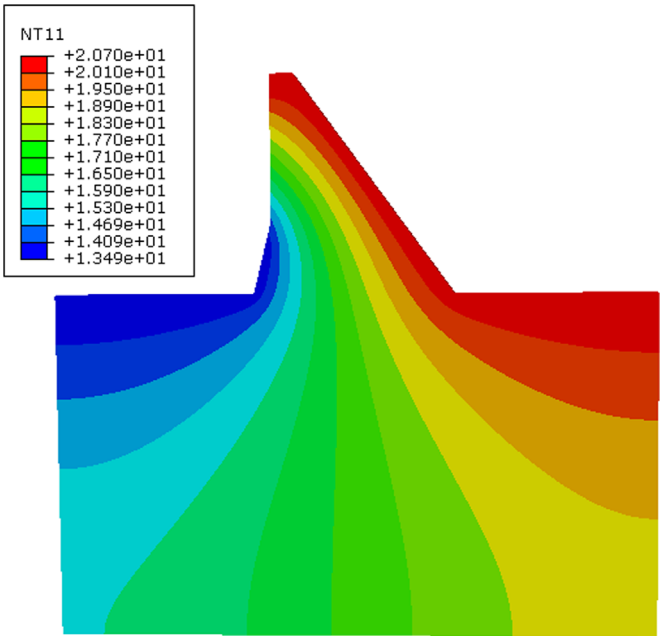

Fig. 13. The thermal state by FEM.

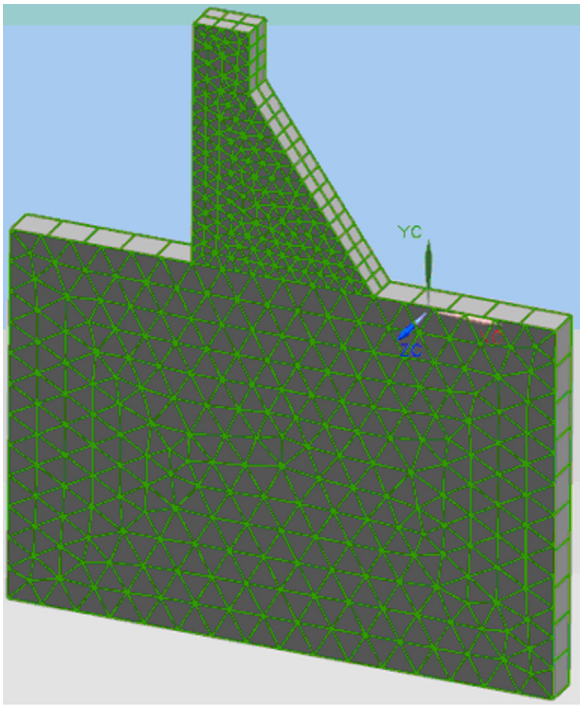

Fig. 14. The BFM mesh.

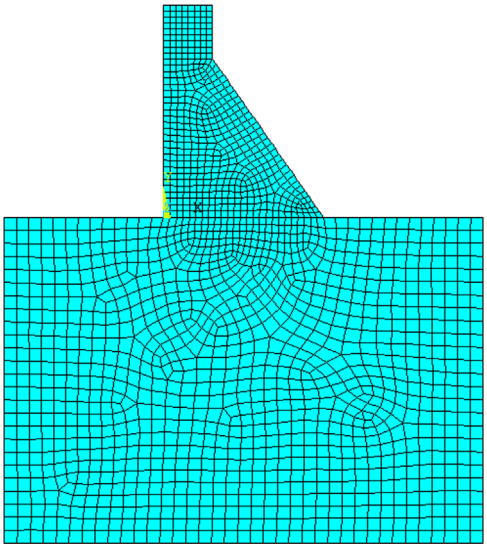

Fig. 15. The FEM mesh.

tools, e.g. ANSYS or ABAQUS. The examples involve steady state heat conduction, transient heat conduction and heat simulation in varying domains (the construction simulation). Results have demonstrated the advantages of the BFM with respect to both accuracy and efficiency.

3.1. Steady state heat conduction in a dam

In old ages, the thermal state in a dam approaches stable. At this stage, the temperature distribution in it can be predicted by a steady state heat conduction analysis. Fig. 11 shows a sliced part of a concrete dam with the width being 20 m. The air temperature is taken as 20.4 °C. The temperature of water is given by

$$T_w = 20.7 - 0.0591572 \times h \tag{3}$$

where h is the depth into the water. All other faces are prescribed as adiabatic boundary condition. The material properties for the dam and base are given in Table 2. In the table c, ρ and κ are the heat capacity, the mass density and the heat conductivity, respectively.

The temperature distribution is shown in Fig. 12. And Fig. 13 shows the results by ABAQUS. It is seen that results by both methods are in very good agreement. However, the BFM computation used totally 29,139 nodes while the FEM computation used 272,300 nodes.

3.2. Transient heat conduction in a dam

This example considers a natural cooling process of a dam shown in Fig. 14. The dam model consists of two parts: the dam body and the base part (the rock foundation). The heat capacity, the mass density and the heat conductivity for both the dam and the foundation are 2539 kg/m^3, 0.888 kJ/(kg °C) and

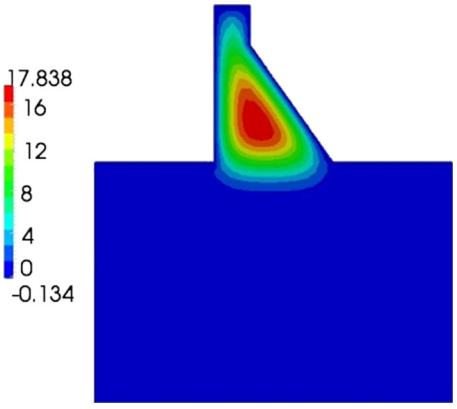

Fig. 16. Thermal state at year 1 by BFM.

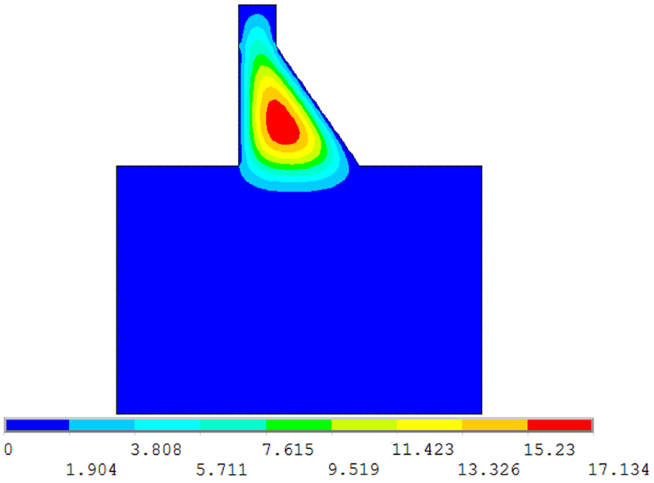

Fig. 17. Thermal state at year 1 by FEM.

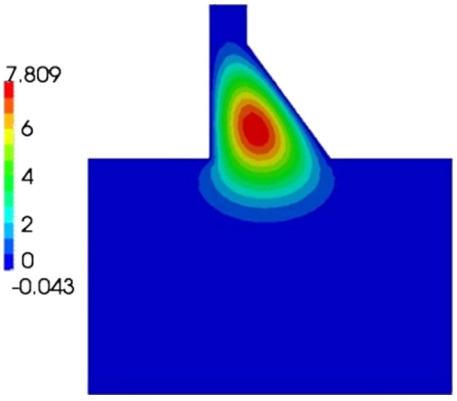

Fig. 18. Thermal state at year 3 by BFM.

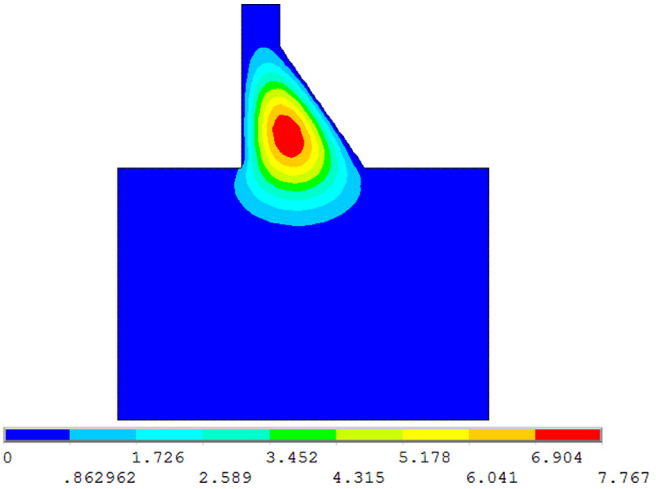

Fig. 19. Thermal state at year 3 by FEM.

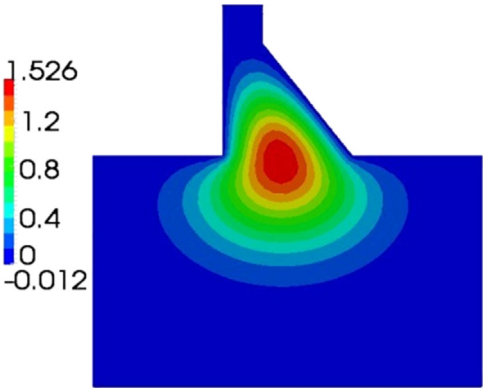

Fig. 20. Thermal state at year 8 by BFM.

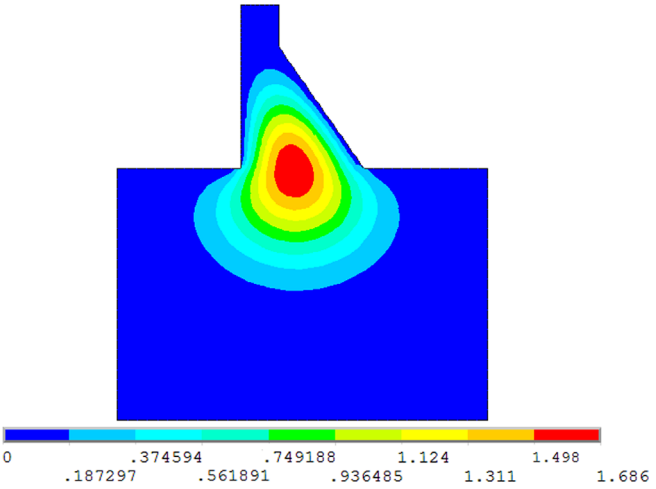

Fig. 21. Thermal state at year 8 by FEM.

9.75 kJ/(m h °C), respectively. The initial temperature for the dam is 20 °C and for the base is 0 °C. The environmental temperature is also 0 °C. The model is discretized with 3896 boundary elements and 2418 nodes. The considered time span is 8 years, which is divided into 384 analysis time steps. For comparison, this problem has also been solved using ANSYS11.0 with 1585 quadrilateral elements in two dimensions (Fig. 15). Temperature distributions at the time points of 1, 3 and 8 years obtained by both methods are compared in Figs. 16–21. Again, the results are in very good agreement with each other.

3.3. *Transient thermal problems involving varying domains*

To simulate the temperature development during a gravity dam's construction process, a transient problem involving varying domains must be solved. This is because a gravity dam is constructed layer by layer. Preparation of FEM input data for such kind of problems could be very complicated. However, the simulation can be automatically carried out by our CAD/CAE unified solution scheme. In the scheme, the geometry model of the multi-layer dam is built in UG-NX, and the layers involved in

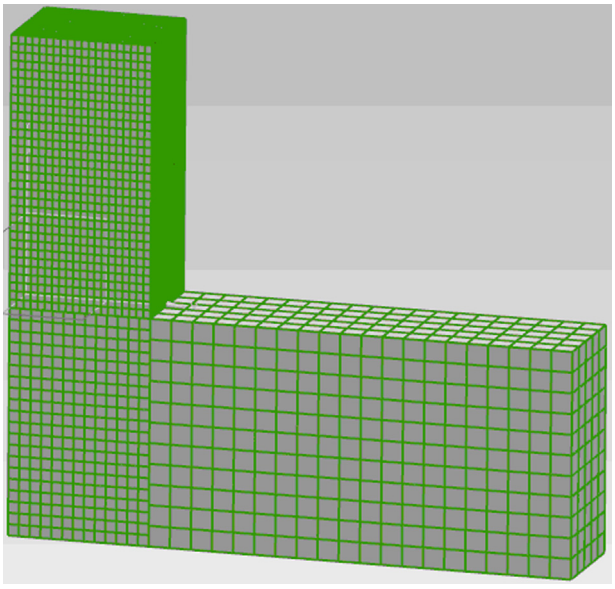

Fig. 22. The BFM mesh for 16 layers.

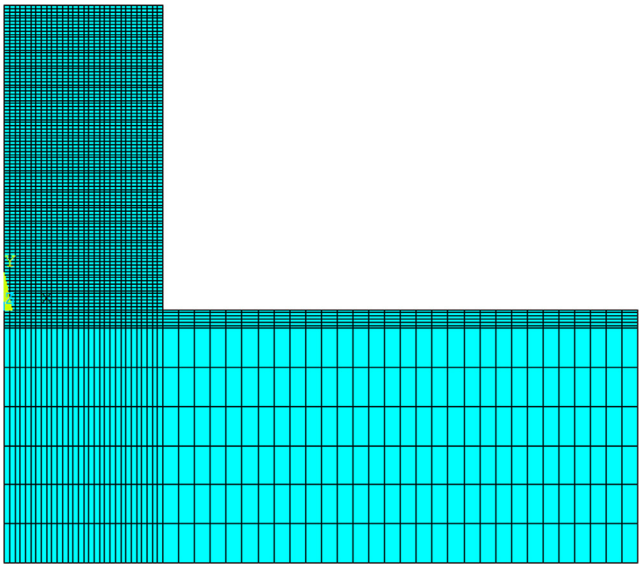

Fig. 23. The FEM mesh for 16 layers.

every analysis step are defined according to the construction schedule. The interfaces between the layers are identified automatically in each analysis step and either the boundary condition or interface condition are also determined and imposed on the surfaces of the layers. An example of a simplified dam model containing 16 layers is considered here to validate our algorithms and solution scheme. To compare with the FEM, the problem has also been solved using ANSYS11.0. In the FEM computation, the model is further simplified into a bi-dimensional problem.

The heat diffusivity and the heat conductivity for both the dam and the base are 0.004 m^2/h and 10 kJ/(m h °C), respectively. The initial temperature for the whole model is 0 °C. The adiabatic temperature rise of the concrete layers is given by

$$\theta(\tau)=\frac{25.0\tau}{4.5+\tau}(^{\circ}C) \tag{4}$$

and the heat source generation rate in the rock foundation is 0. The environmental temperature is also 0 °C. Fixed temperatures

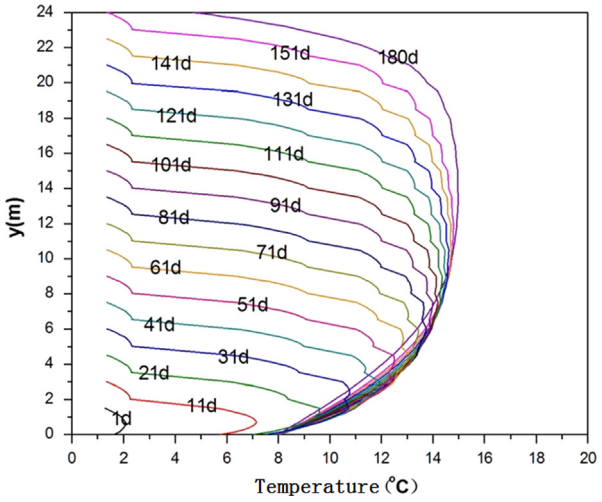

Fig. 24. Temperature variation by BFM.

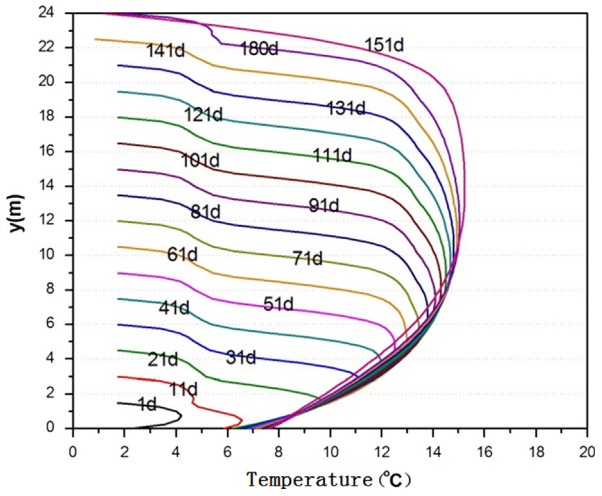

Fig. 25. Temperature variation by FEM.

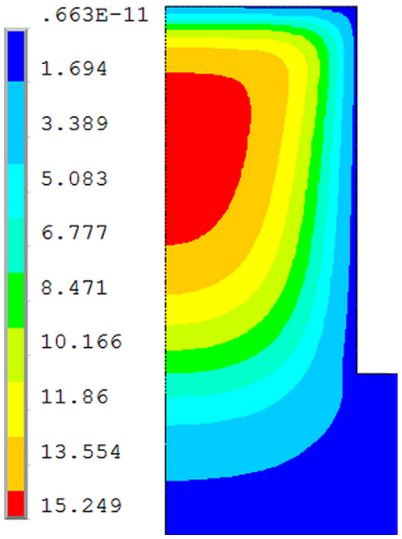

Fig. 26. Thermal state at day 180 by BFM.

taken as the environmental temperature are prescribed on the bottom and right sides of the rock foundation. Adiabatic boundary conditions are imposed on all left side faces of the model. Surfaces

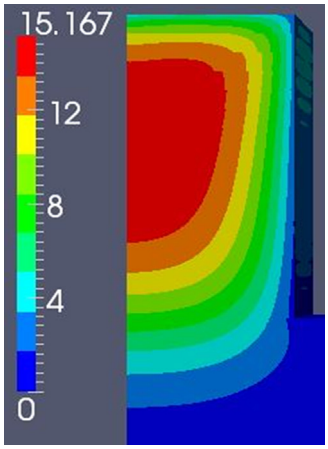

Fig. 27. Thermal state at day 180 by FEM.

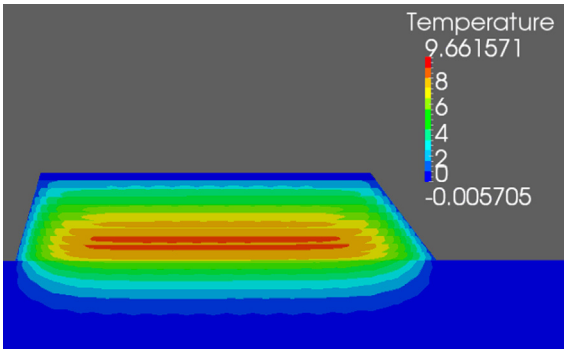

Fig. 28. Thermal state at hour 100.

exposed to atmosphere satisfy the Robin boundary condition

$$\lambda\frac{\partial T}{\partial n} = -\beta(T - T_a) \tag{5}$$

where T_a is the environmental temperature. The convection surface coefficient β takes the value of 60.0 kJ/(m h °C).

The discretized models are show in Figs. 22 and 23. Totally 2379 boundary quadrilateral elements have been used for the BFM computation, and 450 planar quadrilateral elements for the FEM computation. Figs. 24 and 25 represent the temperature variation during the time along the central vertical line on the left side of the model. Figs. 26 and 27 show the thermal state at day 180.

3.4. A real dam simulation

The gravity dam shown in Fig. 11 is considered in the present analysis. The dam is divided into 62 layers according to its construction schedule. The characteristics, such as materials, boundary and initial conditions, the hydration heat of the cement are taken as the example described in Section 3.3. The simulation consists of 60 sequential analyses, which are further subdivided into 1260 time steps, and span totally 76,500 h. For the simulation, 5827 boundary quadrilateral elements with 24,527 nodes and 5360 hexahedron volume elements with 36,327 internal nodes have been used. The entire computation is finished within 2107s (with domain number sequence optimization). Figs. 28–33 show the temperature distribution in the dam body at the considered time. For further details and animation of the temperature development, see the web site: www.5aCAE.com.

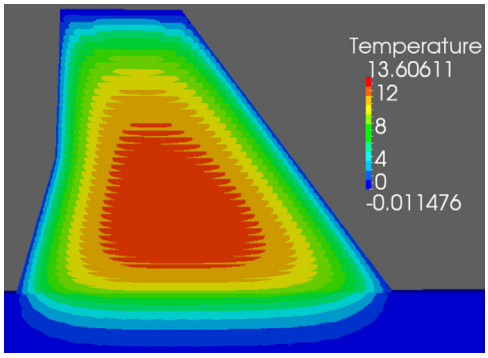

Fig. 29. Thermal state at hour 400.

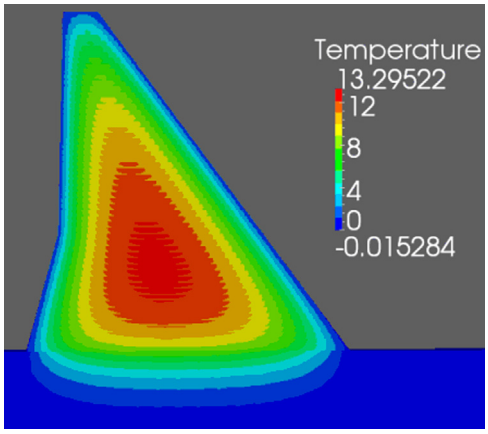

Fig. 30. Thermal state at hour 900.

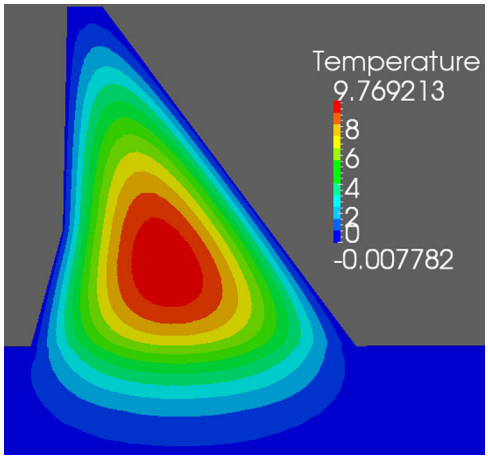

Fig. 31. Thermal state at hour 3000.

4. Conclusion

In this work, the boundary face method is applied in the computation of the temperature in gravity dams with heat generation due to hydration of concrete. The BFM has been seamlessly integrated into a CAD package (here the NX-UG has been chosen), making the thermal analysis can be automatically conducted and completely within the CAD environment. All the characteristics of analysis, such as the material properties, boundary and initial conditions, heat sources etc., are applied to the geometry entities naturally with the CAD tools, rather than to elements or nodes.

Bench mark examples with comparison with some mature FEM packages (e.g. ABAQUS and ANSYS) are presented. It has been demonstrated that our method is able to get high accuracy

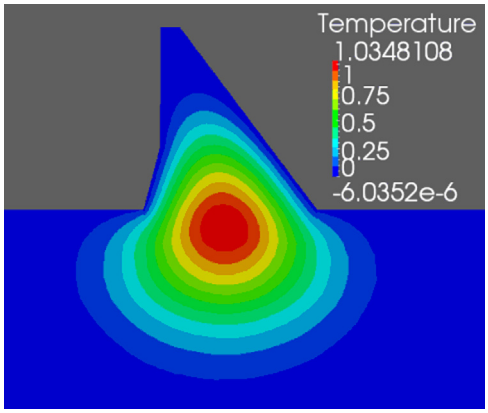

Fig. 32. Thermal state at hour 20,000.

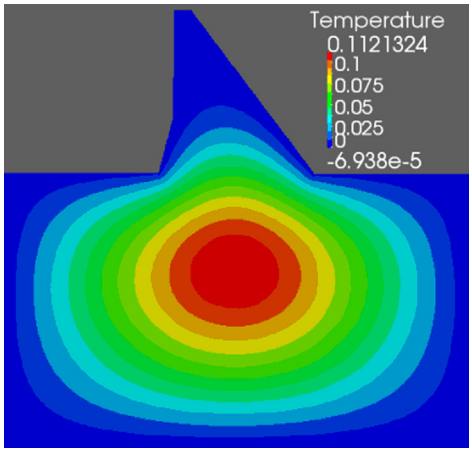

Fig. 33. Thermal state at hour 76,500.

equivalent to the FEM but with lower cost in terms of both human labour and computational resources.

This work has not been finished yet. Thermal stress analysis using an elasto-visco-plastic model and taking into account the rheology of the concrete from very young to old ages is still ongoing.

Acknowledgements

This work was supported in part by National Science Foundation of China under Grant number 11172098 and in part by National 973 Project of China under Grant number 2010CB328005.

References

[1] 5aCAE, ⟨http://www.5acae.com⟩.
[2] Zhang JM, Qin XY, Han X, Li GY. A boundary face method for potential problems in three dimensions. Int J Numer Methods Eng 2009;80(3):320–37.
[3] Qin XY, Zhang JM, Li GY, Sheng XM, Song Q, Mu DH. An element implementation of the boundary face method for 3D potential problems. Eng Anal Boundary Elem 2010;34:934–43.
[4] Brebbia CA, Telles JCF, Wrobel LC. Boundary element techniques. Berlin and New York: Springer-Verlag; 1984.
[5] Cheng AHD, Cheng DT. Heritage and early history of the boundary element method. Eng Anal Boundary Elem 2005;29(3):268–302.
[6] Chen JT, Lin SR, Chen KH. Degenerate scale problem when solving Laplaces equation by BEM and its treatment. Int J Numer Methods Eng 2005;62(2):233–61.
[7] Dong CY, Lee KY. Boundary element analysis of infinite anisotropic elastic medium containing inclusions and cracks. Eng Anal Boundary Elem 2005;29(6):562–9.
[8] Niu ZR, Zhou HL. The natural boundary integral equation in potential problems and regularization of the hypersingular integral. Comput Struct 2004;82(2):315–23.
[9] Zhang J, Zheng X, Lu CJ, Xie GZ, Li GYA. Geometric mapping cross approximation method. Eng Anal Boundary Elem 2013;37(12):1668–73.
[10] Huang C, Zhang JM, Qin XY, Lu CJ, Sheng XM, Li GY. Stress analysis of solids with open-ended tubular holes by BFM. Eng Anal Boundary Elem 2012;36:1908–16.
[11] Qin XY, Zhang JM, Liu LP. Steady-state heat conduction analysis of solids with small open-ended tubular holes by BFM. Int J Heat Mass Transfer 2012;55:6846–53.
[12] Zhou FL, Xie GZ, Zhang JM. Transient heat conduction analysis of solid with small open-ended tubular cavities by boundary face method. Eng Anal Boundary Elem 2013;37:542–50.
[13] Wang XH, Zhang JM, Zhou FL, Zheng XS. An adaptive fast multipole boundary face method with higher order elements for acoustic problems in three-dimension. Eng Anal Boundary Elem 2013;37:114–52.
[14] Henry DP, Banerjee PK. Elastic analysis of three-dimensional solids with small holes by BEM. Int J Numer Methods Eng 1991;31:369–84.
[15] Qin QH, Wang H. Special circular hole elements for thermal analysis in cellular solids with multiple circular holes. Int J Comput Methods 2013;10:04.
[16] Wang H, Qin QH. A new special element for stress concentration analysis of a plate with elliptical holes. Acta Mech 2012;223(6):1323–40.
[17] Wang H, Qin QH. Fundamental-solution-based hybrid FEM for plane elasticity with special elements. Comput Mech 2011;48(5):515–28.
[18] Yao ZH, Kong FZ, Wang HT, Wang PB. 2D simulation of composite materials using BEM. Eng Anal Boundary Elem 2004;28(8):927–35.
[19] Liu YJ. A fast multipole boundary element method for 2D multi-domain elastostatic problems based on a dual BIE formulation. Comput Mech 2008;42(5):761–73.
[20] Gao XW, Guo L, Zhang C. Three-step multi-domain BEM solver for nonhomogeneous material problems. Eng Anal Boundary Elem 2007;31(12):965–73.
[21] Zhang JM, Li Y, Lu CJ, Han L, Li GY. A domain renumbering algorithm for multi-domain boundary face method. Eng Anal Boundary Elem, submitted for publication.
[22] Hackbusch W, Nowak ZP. On the fast matrix multiplication in the boundary element method by panel clustering. Numerische Math 1989;54:463–91.
[23] Bebendorf M, Rjasanov S. Adaptive low-rank approximation of collocation matrices. Computing 2003;70(1):1–24.
[24] Rokhlin V. Rapid solution of integral equations of classical potential theory. J Comput Phys 1985;60:187–207.
[25] Zhang JM, Masa Tanaka, Endo M. The hybrid boundary node method accelerated by fast multipole method for 3-D potential problems. Int J Numer Methods Eng 2005;63:660–80.
[26] Zhang JM, Tanaka Masa. Adaptive spatial decomposition in fast multipole method. J Comput Phys 2007;226(1):17–28.
[27] Zhang JM, Tanaka Masa. Systematic study of thermal properties of CNT composites by a fast multipole hybrid boundary node method. Eng Anal Boundary Elem 2007;31:388–401.
[28] Zhang JM, Zhuang C, Qin XY, Li GY, Sheng XM. FMM-accelerated hybrid boundary node method for multi-domain problems. Eng Anal Boundary Elem 2010;34:433–9.
[29] Zhou FL, Li XH, Zhang JM, Huang C, Lu CJ. A time step amplification method in boundary face method for transient heat conduction. Int. J Heat Mass Transfer, submitted for publication.